ACTA ACUSTICA UNITED WITH ACUSTICA
Vol. 89 (2003) 1025 – 1037

Acoustics of 90 degree sharp bends. Part I: Low-frequency acoustical response

S. Dequand*, S. J. Hulshoff**, Y. Aurégan***, J. Huijnen*, R. ter Riet*, L. J. van Lier*, A. Hirschberg*
*: Technische Universiteit Eindhoven, Postbus 513, 5600 MB Eindhoven, The Netherlands
**: Faculty of Aerospace Engineering, Delft Univ. of Technology, Kluyverweg 1, 2629HS Delft, The Netherlands
***: Laboratoire d'Acoustique de l'Université du Maine, UMR-CNRS 6613, Université du Maine, Av. Olivier Messiaen, 72085 Le Mans Cedex 09, France

Summary
The *acoustical* response of 90 degree sharp bends to acoustical perturbations in the absence of a main flow is considered. The *aeroacoustical* response of these bends is presented in part II [1]. The bends considered have a sharp 90 degree inner edge and have either a sharp or a rounded outer corner. They are placed in pipes with either a square cross-section (2D-bends) or a circular cross-section (3D-bends). The acoustical performance of a numerical method based on the non-linear Euler equations for two-dimensional inviscid and compressible flows is checked and its ability to predict the response of 3D-bends is investigated. The comparison between 2-D and 3-D data is made for equal dimensionless frequencies f/f_c where f is the frequency of the acoustical perturbations and f_c is the cut-off frequency of the bends. In the case of a bend with a sharp inner edge and a sharp outer corner, the 2-D numerical predictions agree with 2-D analytical data obtained from a mode expansion technique and with 2-D experimental data from literature and our own 3-D experimental results. In the case of a bend with a sharp inner edge and a rounded outer corner, the 2-D numerical simulations predict accurately the 2-D experimental data from literature. However, the 2-D numerical predictions do not agree with our 3-D experimental data. The acoustical response of 3D-bends appears to be independent of the shape of the outer corner. This behavior is quite unexpected.

PACS no. 43.20.Mv, 43.20.Ra, 43.20.Fn

1. Introduction

Bends are common in pipe systems. They are often used to keep long devices, as encountered in gas-transport systems or in wind musical instruments, reasonably compact.

The acoustical effect of the presence of a bend in a pipe with a square cross-section has been investigated by Rostafinski [2, 3, 4], Cummings [5] and Félix [6]. Analytical models to predict the acoustic wave scattering in a sharp bend have been proposed as early as 1947. Miles [7] proposed a transmission line approach (equivalent to a modal analysis). Lippert [8] compared his experimental results with a single mode approximation of Miles' theory [7]. Thompson [9] and Bruggeman [10] used a matched asymptotic expansion technique. At low frequencies, this matched asymptotic method reduces to the calculation of the incompressible potential flow in the bend, which can be done by means of conformal mapping. As explained by Bruggeman [10], this approach provides a much better description of the flow near edges than a mode expansion method.

This paper is devoted to a test of a numerical method[1] based on the non-linear Euler equations for two-dimensional inviscid and compressible flow and the question whether such a method can be used to predict the response of more complex three-dimensional bends and the effect of a main flow on this response. In this paper the acoustical performance of the method for a quiescent uniform reference state of the fluid is checked. Numerical predictions of the aeroacoustical behavior of bends, that is their response to acoustical waves in the presence of a main flow, are presented in a companion paper (part II [1]). Different methods are used to extract far-field information from numerical results. An extraction method which determines the one-dimensional acoustic waves by means of a Fast Fourier Transform of the time-dependent pressure and velocity signals can be used. The second method of extraction is based on an integral formulation. Comparison between the results obtained by means of the two methods provides insight into the accuracy of our calculations.

In practice, most pipes have circular cross sections, and the bend flow is not two-dimensional. Bends in pipes with

Received 11 June 2002,
accepted 10 June 2003.

[1] The EIA code ('Euler code for Internal Aeracoustics') was developed by Hulshoff in the framework of the European project Flodac (BRPR CT97-0394).

© S. Hirzel Verlag · EAA

circular cross-sections have been studied by Keefe and Benade [11]. They measured the inertance and the transition correction between the bend and the straight pipe. Félix [12] presents results obtained by means of a mode expansion method. Nederveen [13] calculated the inertance change in a 3D-bend by decomposing the cross-section of the bend into parallel (independent) thin layers, that is a decomposition in parallel 2D-bends. By integration over the cross-sectional area of the 3D-bend, he obtained a prediction of the inertance in the limit of low frequencies for bends with a radius of curvature $r \geq 0.6D$ (where D is the pipe diameter and r is the radius of curvature taken on the pipe axis). His results are in good agreement with 3-D numerical calculations and experimental results. Our aim is to further explore the validity of such an approach. The particular case of a bend with a sharp inner edge is considered. This corresponds to a radius of curvature $r = D/2$.

Another possibility of using two-dimensional models as approximate solutions for such 3-D configurations is also explored. 2-D and 3-D data are assumed to correspond to each other for equal dimensionless frequency f/f_c. The 2-D numerical data are compared to our own 3-D experimental data obtained by measuring the response of bends with circular cross sections. The measurements have been carried out by means of a two-source method. This method is described by Åbom [14], Ajello [15] and Durrieu [16]).

Figure 1 shows a scheme of the bends considered. They all have a sharp 90 degree inner edge and are placed in pipes with either a square cross-section (2D-bends) or a circular cross-section (3D-bends). Strictly speaking, the data for pipes with a square cross-section are three-dimensional but they are expected to be accurately described by a two-dimensional theory. Bends in such pipes are therefore referred as 2D-bends in comparison with bends in pipes with circular cross-section (3D-bends). For each type of pipes, bends with either a sharp or a rounded outer corner are considered. The aeroacoustical response of these configurations in the presence of a main flow will be considered in a companion paper (part II [1]). The turbulence noise production of the same bends is discussed by Gijrath [17] and Nygård [18]. The work of Nygård [18] includes the effect of the interaction between two successive bends on turbulent noise production.

Our study is restricted to the acoustic response of the bends at frequencies f below the cut-off frequency f_c. This implies that only plane waves propagate along the pipe segments 1 upstream and 2 downstream of the bends (Figure 1). Under these circumstances, it is convenient to express the bend response in terms of the scattering matrix [14] defined in section 2.

The acoustical response of 90° bends with a sharp inner edge in a pipe with square cross sections (bend A and bend B, Figure 1) has been measured by Lippert [8]. For the 90° bend with a sharp inner edge and a sharp outer corner, the acoustical response is predicted by means of the mode expansion proposed by Miles [7]. We use more modes than the single mode approximation used by Lippert [8]. This provides a better approximation of the exact solution.

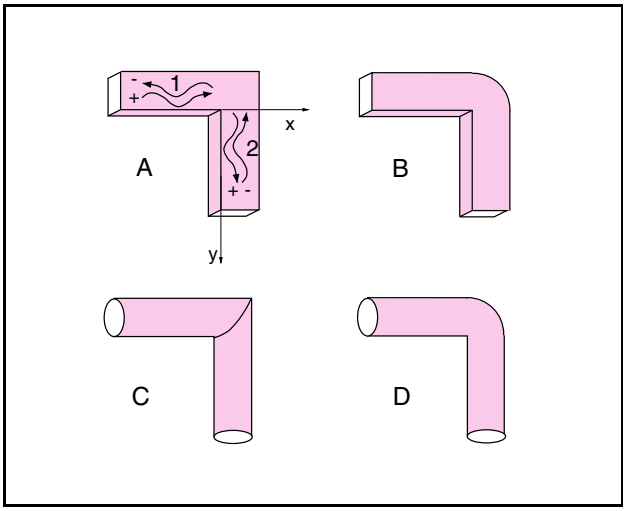

Figure 1. 90 degree sharp-edged bends considered in the study. Bend A: Bend with a sharp inner edge and a sharp outer corner (square cross sections); Bend B: Bend with a sharp inner edge and a rounded outer corner (square cross sections) ($r = D/2$); Bend C: Bend with a sharp inner edge and a sharp outer corner (circular pipes); Bend D: Bend with a sharp inner edge and a rounded outer corner (circular pipes) ($r = D/2$). Note the convention chosen for the axis direction and the reference planes for the determination of the phases (planes $x = 0$ for the pipe segment 1 and $y = 0$ for the pipe segment 2).

Theoretical models are described in section 2. The numerical method is presented in section 3. The experimental method for measurements of the response of the 3-D bends is described in section 4. In section 5, the experimental data of Lippert [8] are compared to 2-D numerical and theoretical data and finally, 3-D experimental data are presented.

2. Theory

2.1. Definitions

2.1.1. Cut-off frequency f_c

For pipes with circular cross-sections, the cut-off frequency f_c below which only plane waves propagate is

$$f_c = \varsigma \frac{c_0}{\pi D}, \tag{1}$$

where $c_0 = 343.2042$ m/s is the speed of sound for dry air at room temperature $T^o = 293.15$ K and D is the pipe diameter. The coefficient $\varsigma = 1.8412\ldots$ is the smallest non-zero eigenvalue (zero of the ordinary Bessel function of the first kind) which corresponds to the first evanescent mode in a pipe with circular cross-sections [19]. In our case, the 3-D bends have a pipe diameter of 0.03 m, so that the cut-off frequency is $f_c \approx 6.7$ kHz.

For pipes with square cross-sections $D \times D$, the cut-off frequency is simply $f_c = c_0/2D$.

2.1.2. Scattering matrix $\mathcal{S}$

Below the cut-off frequency ($f < f_c$), the response of a bend to an acoustical perturbation can be expressed in terms of the scattering matrix $\mathcal{S}$ [14]:

$$\begin{pmatrix} p_2^+ \\ p_1^- \end{pmatrix} = \underbrace{\begin{pmatrix} T_p^+ & R_p^- \\ R_p^+ & T_p^- \end{pmatrix}}_{\mathcal{S}} \begin{pmatrix} p_1^+ \\ p_2^- \end{pmatrix}, \tag{2}$$

where p_1^+ and p_2^- are the amplitudes of the upstream and downstream incoming waves, respectively. The scattered waves have the amplitudes p_2^+ and p_1^-. The pressure wave reflection coefficient R_p^+ and the transmission coefficient T_p^+ correspond to the reflection and transmission of p_1^+ when the downstream pipe segment is anechoic so that $p_2^- = 0$. They are called the upstream anechoic reflection and transmission coefficients. The coefficients R_p^- and T_p^- have a similar physical interpretation and are called the downstream anechoic reflection and transmission coefficients.

In the absence of a main flow ($\overline{u_1} = 0$), the scattering matrix (equation 2) is symmetric:

$$R_p^+ = R_p^- = R_p = |R_p| \mathrm{e}^{\mathrm{j}\Phi_R}, \tag{3}$$

$$T_p^+ = T_p^- = T_p = |T_p| \mathrm{e}^{\mathrm{j}\Phi_T}, \tag{4}$$

where Φ_R and Φ_T are the phases of the reflection and the transmission coefficients, respectively. The reference planes for determining the origin of the phases are the planes $x = 0$ for Φ_R and $y = 0$ for Φ_T, respectively, as shown in Figure 1.

Furthermore, if visco-thermal losses are neglected, the energy conservation law yields:

$$|R_p|^2 + |T_p|^2 = 1. \tag{5}$$

In this case (when $\overline{u_1} = 0$), only two equations are needed to determine the coefficients of the scattering matrix.

2.2. Miles' theory

Miles [7] proposed a modal expansion method to predict the acoustical behavior of a bend in a pipe with square cross-section $D \times D$. The acoustical pressure in the straight upstream ($i = 1$) and downstream ($i = 2$) pipes can, for harmonic waves of frequency $\omega = 2\pi f$, be expressed as the sum of contributions of straight pipe modes:

$$p_1(x,y) = \sum_m \sqrt{\frac{2-\delta_{m0}}{D}} \cos\left(\frac{m\pi y}{D}\right) \cdot \left[A_{m1}\mathrm{e}^{-\mathrm{j}k_m x} + B_{m1}\mathrm{e}^{\mathrm{j}k_m x}\right], \tag{6}$$

$$p_2(x,y) = \sum_m \sqrt{\frac{2-\delta_{m0}}{D}} \cos\left(\frac{m\pi x}{D}\right) \cdot \left[A_{m2}\mathrm{e}^{-\mathrm{j}k_m y} + B_{m2}\mathrm{e}^{\mathrm{j}k_m y}\right], \tag{7}$$

where D is the height of the pipes, δ_{m0} is the Kronecker tensor, k_m represent the wave numbers for each mode m ($k_m = \sqrt{(\omega/c_0)^2 - (m\pi/D)^2}$). We use here a $\mathrm{e}^{\mathrm{j}\omega t}$-convention. By writing the mode expansion of the square cavity formed by the junction of the two straight pipes and by equalizing the acoustical pressure at each junction, the coefficients of the scattering matrix can be found [20]. Lippert [8] compared his experimental data to the results of a mode expansion truncated after the first mode. The mode expansion was calculated with a larger number of modes and a convergence of the results was found within 0.1% above ten modes. These results are compared to the experimental results of Lippert [8] in Figures 2 and 3. These figures show that increasing the number of modes improves the correlation with experimental data.

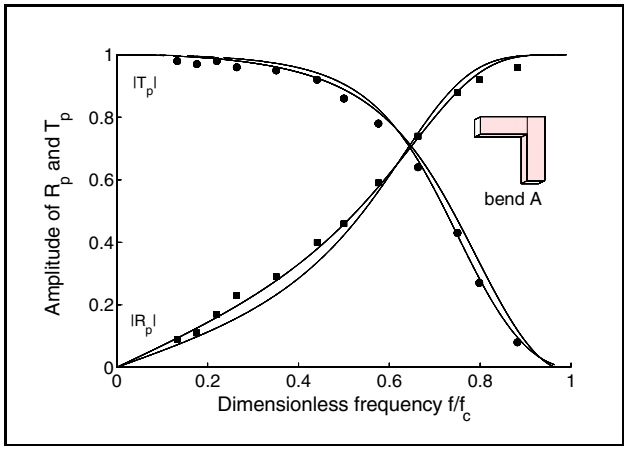

Figure 2. Bend A (2D-bend with a sharp inner edge and a sharp outer corner): Amplitude of the pressure wave reflection and transmission coefficients as a function of the dimensionless frequency f/f_c. Comparison between the experimental data of Lippert [8] (■, ●) and the analytical solutions based on a mode expansion truncated after 1 mode (— — —) and after 10 modes (———).

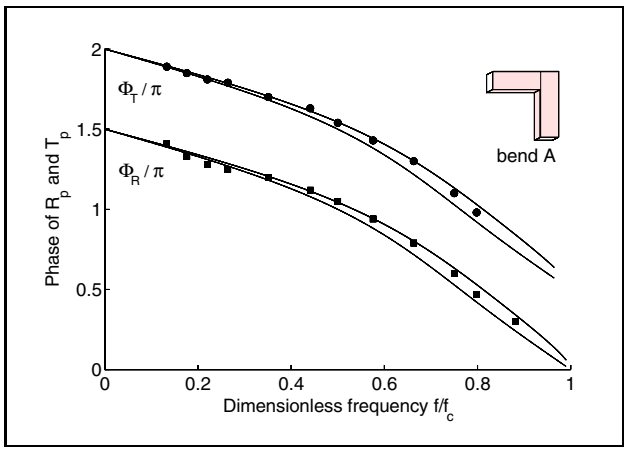

Figure 3. Bend A (2D-bend with a sharp inner edge and a sharp outer corner): Phase of the pressure wave reflection and transmission coefficients as a function of the dimensionless frequency f/f_c. Comparison between the experimental data of Lippert [8] (■, ●) and the analytical solutions based on a mode expansion truncated after 1 mode (— — —) and after 10 modes (———).

2.3. From 2-D bends to 3-D bends

Nederveen [13] calculated the inertance of a 3D-bend by decomposing the cross-section of the bend into parallel 2D-bends.

This decomposition of a 3D-bend into parallel thin layers is applied in our study to determine the magnitude of the reflection and transmission coefficients of a 3D-bend from the coefficients of 2D-bends. The cross-section of the 3D-bend is cut into parallel thin rectangular layers such that the total surface of these rectangles is equal to the cross-sectional area S_p of the 3D-bend. For each thin layer (2D-bend), the cut-off frequency $f_c^{(i)}$ is calculated and the amplitude of the reflection and transmission coefficients can be deduced from the 2-D results as a function of the dimensionless frequency $f/f_c^{(i)}$. By using an electro-acoustic analogy, a 2D-bend can be represented by an equivalent electric network. Assuming that there is no lateral flow between these bends, the system of N parallel thin layers is then equivalent to a global electric network consisting of N of these electric networks connected in parallel. A simple relationship between the different elements of the system can be written and corresponds to the continuity of pressure and velocity:

$$\begin{cases} S_p u_1 = \sum_{i=1}^{N} S_p^{(i)} u_1^{(i)}, \\ S_p u_2 = \sum_{i=1}^{N} S_p^{(i)} u_2^{(i)}, \\ \quad p_1 = p_1^{(i)} \qquad\qquad \forall\, \mathrm{i}, \\ \quad p_2 = p_2^{(i)} \qquad\qquad \forall\, \mathrm{i}, \end{cases} \tag{8}$$

where S_p is the circular cross-sectional area of the 3D-bend, $S_p^{(i)}$ is the cross-section area of each thin layer i, u_1 and u_2 are the incoming and the outgoing velocity of the 3D-bend, $u_1^{(i)}$ and $u_2^{(i)}$ are the incoming and outgoing velocity of a thin layer i, p_1 and p_2 are the pressures in the upstream and downstream pipe segments of the 3D-bend, $p_1^{(i)}$ and $p_2^{(i)}$ are the pressures in the upstream and downstream pipe segments of a thin layer i.

Figures 4 and 5 show the amplitude and the phase of the reflection and transmission coefficients as a function of the dimensionless frequency f/f_c for bends with a sharp outer edge (Figure 4) and with a rounded outer corner (Figure 5). The results obtained by means of the decomposition in 2D parallel bends are compared to the 2D theoretical results obtained using the numerical method as described in section 3. For a bend with a sharp outer corner (Figure 4), the amplitude predicted by the analytical model only differs slightly from the amplitude predicted numerically for the 2-D bends. The predicted phase of the 3-D coefficients is larger than the 2-D theoretical value. At high frequencies ($f/f_c > 0.65$), a problem of numerical instabilities occurs and the analytical model could not easily be used to predict the amplitude and the phase of the reflection and transmission coefficients. This problem does not occur in the case of a bend with a rounded outer corner (Figure 5). At low frequencies ($f/f_c < 0.4$), the amplitude of the reflection and transmission coefficients calculated by means of this intuitive approach is equal to the amplitude of the reflection and transmission coefficients of a 2D-bend predicted by numerical computations (Figure 4). At higher frequencies, the predicted 3-D reflection coefficient becomes larger than its 2-D value.

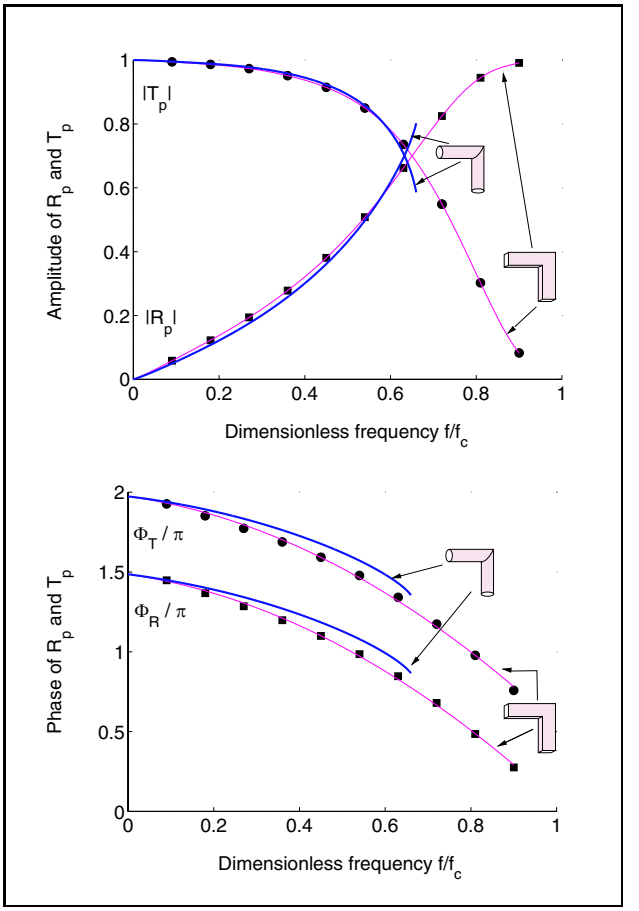

Figure 4. Bend with a sharp outer corner. Amplitude and phase of the pressure wave reflection and transmission coefficients R_p and T_p in terms of the dimensionless frequency f/f_c. Comparison between the analytical data obtained by means of the decomposition into 2D-bends (———) and 2D numerical simulations (the numerical method is described in section 3) (●, ■).

3. Numerical method

3.1. Approach

Numerical simulations were performed using the numerical method based on the two-dimensional non-linear Euler equations for inviscid and compressible flows [21]. The spatial discretization method was based on a second-order cell-centered finite-volume method. For the time integration, a second-order four-stage (low storage) Runge-Kutta method was used.

The Euler equations accurately represent the propagation of acoustic waves. Elementary tests of the code are provided by Hulshoff [21] and Dequand [22].

The far-field acoustic response of the bends can be extracted from the 2-D flow simulation using two differ-

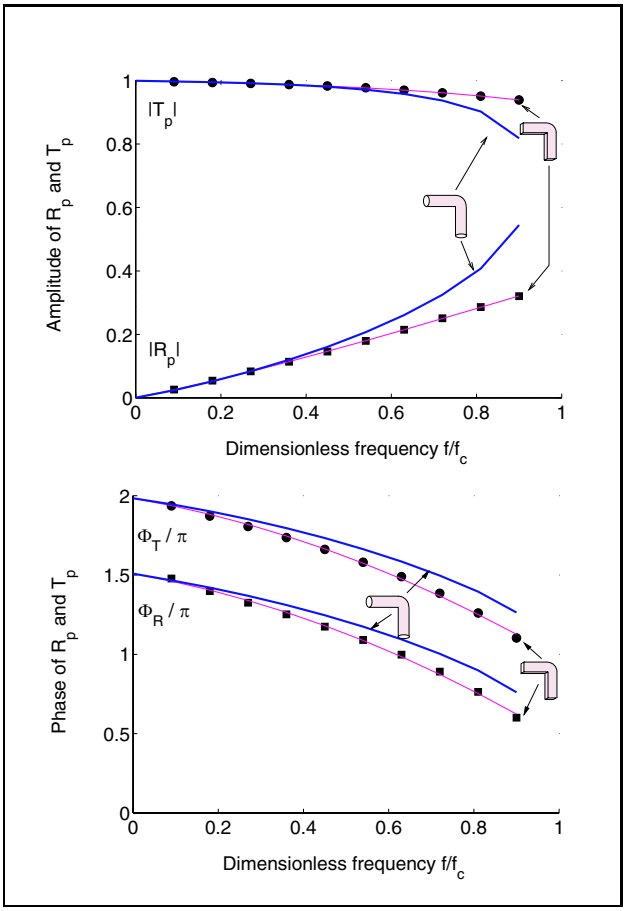

Figure 5. Bend with a rounded outer corner. Amplitude and phase of the pressure wave reflection and transmission coefficients R_p and T_p in terms of the dimensionless frequency f/f_c. Comparison between the analytical data obtained by means of the decomposition into 2D-bends (———) and the 2D numerical simulations (the numerical method is described in section 3) (●, ■).

ent approaches: a 1-D extraction procedure or an integral method. Comparison of the results obtained by means of these two different extraction methods provides some insight into the accuracy of the numerical results. The energy conservation (equation 5) is used as an additional test.

3.2. Post-processing

3.2.1. 1-D extraction

Figure 6 shows a sketch of the numerical domain used for the computations of the acoustic response of the bend with a sharp outer corner (Bend A, Figure 1).

The numerical domain consists of two-dimensional blocks in which the Euler equations are solved and one-dimensional blocks within which information from the 2-D domain is transferred.

The Euler equations can be written in an integral conservation form:

$$\frac{\partial}{\partial t}\int_V W \,\mathrm{d}V + \int_S \boldsymbol{F}\cdot\boldsymbol{n}\,\mathrm{d}S = 0, \tag{9}$$

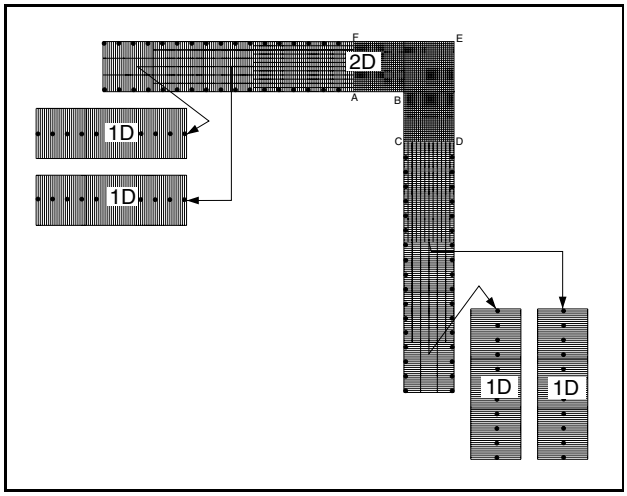

Figure 6. Scheme of the numerical domain used for the 2-D Euler computations. 2-D blocks are connected to 1-D blocks for the extraction procedure and numerical 'probes' (●) are placed at user-specified locations in the domain.

where V is the volume and S is the surface of the domain, and $\boldsymbol{n}$ is the unit vector normal and outwards to the surface. W represents the conservative variables:

$$W = \begin{bmatrix} \rho \\ \rho\boldsymbol{u} \\ \rho E \end{bmatrix}, \tag{10}$$

where ρ is the density, E is the total energy per unit mass, $\boldsymbol{u}$ is the fluid velocity. In the set of equations 9, $\boldsymbol{F}\cdot\boldsymbol{n}$ represents the normal component of the fluxes through the surface of the control volume V and is expressed as:

$$\boldsymbol{F}\cdot\boldsymbol{n} = \begin{bmatrix} \rho(\boldsymbol{u}\cdot\boldsymbol{n}) \\ \rho\boldsymbol{u}(\boldsymbol{u}\cdot\boldsymbol{n}) + p\boldsymbol{n} \\ \rho e(\boldsymbol{u}\cdot\boldsymbol{n}) + p(\boldsymbol{u}\cdot\boldsymbol{n}) \end{bmatrix}, \tag{11}$$

where p is the pressure and the internal energy e is related to the total energy by : $E = e + \frac{1}{2}u^2$.

The numerical domain (Figure 6) has also one-dimensional blocks. Such a 1-D block is an extraction region within which information from the 2-D domain is transferred. The extraction is conservative, which means that the sum of fluxes $\boldsymbol{F}$ in the actual pipe cross-section corresponds to the flux imposed on the boundary of the 1-D region. The extraction procedure is also passive, which means that information is only transferred in one direction from 2-D regions to 1-D regions. Therefore, the solution of the 2-D domain is unaffected by the procedure.

The time variation of the pressure $p'(t)$ and the velocity $u'(t)$ perturbation signals are recorded at user-specified points which are called numerical 'probes'. The transient signal before the sinusoidal behavior sets in was typically four periods. The magnitude and the phase of the waves are determined by means of a Fast Fourier Transform of the temporal signals (over ten periods). The positive and negative waves p_i^+ and p_i^- are then deduced from p_i' and u_i' using D'Alembert's solution for 1-D wave propaga-

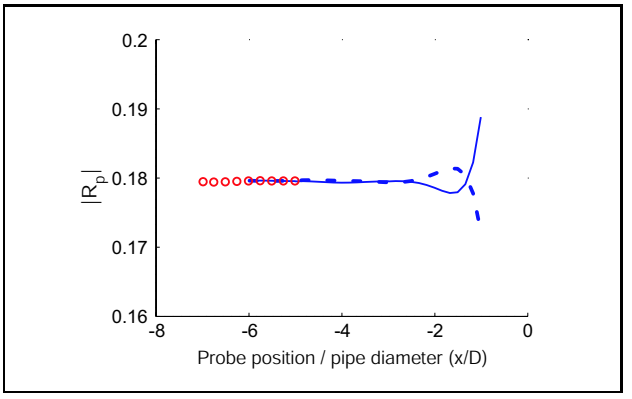

Figure 7. Amplitude of the reflection coefficient $|R_p|$ of the 2-D (inner wall – – – – –, outer wall ———) and 1-D (○) as a function of the probe positions x divided by the pipe diameter D (Bend B (sharp inner edge and rounded outer wall), $\overline{u_1} = 0$, $f/f_c = 0.54$).

tion. In the absence of a main flow, the scattering matrix is symmetric (equation 3 and 4, section 2.1.2) and only two coefficients R_p and T_p have to be determined. A right-travelling acoustic velocity wave (with an amplitude $10^{-3} \times c_0$) is applied at the inlet and an anechoic condition is applied at the outlet of the numerical domain. The coefficients T_p and R_p are then determined from the results of a single numerical calculation.

Figure 7 shows the magnitude of the reflection coefficient $|R_p|$ as a function of the probe positions x in the 2-D and 1-D regions. The origin of the coordinates ($x = 0$) is chosen at the inner edge of the bend. Figure 7 shows that the far-field identification has to be done at least three pipe diameters upstream of the bend. In the region closer to the bend, the acoustical field is two-dimensional. This is deduced from the significant difference of the results observed for the probes placed along the inner bend wall compared to the results obtained for the probes placed at the outer wall. In the absence of a main flow, the presence of 1D blocks is not necessary for the identification of the far-field acoustic response of the bends. Figure 7 shows indeed that, sufficiently far from the bend, the acoustic field becomes one-dimensional. The 1-D extraction procedure by means of additional 1D blocks will be however useful for the determination of the aeroacoustic response of the bends in the presence of a main flow (part II [1]).

3.2.2. Integral method

As a test for the accuracy of the wave propagation calculations and the numerical 1-D extraction method, the coefficients of reflection R_p and transmission T_p are now deduced from the numerical calculations by using an integral method [23].

Lighthill's equation is an exact result derived from the mass and momentum conservation laws (the Navier-Stokes equations):

$$\frac{\partial^2 \rho'}{\partial t^2} - c_0^2 \frac{\partial^2 \rho'}{\partial x_i^2} = \frac{\partial^2 T_{ij}}{\partial x_i \partial x_j}. \tag{12}$$

T_{ij} is the Lighthill stress tensor defined by:

$$T_{ij} = \rho u_i u_j + (p' - c_0^2 \rho')\delta_{ij} - \tau_{ij}, \tag{13}$$

where δ_{ij} is the Kronecker symbol, τ_{ij} is the viscous stress tensor which is neglected further. The prime quantities p' and ρ' represent the deviations of the pressure and the density from the quiescent reference state (ρ_0, p_0) at the observer's position:

$$p' = p - p_0, \tag{14}$$
$$\rho' = \rho - \rho_0. \tag{15}$$

The speed of sound c_0 is also chosen to be that of the fluid at the reference state $c_0 = c(\rho_0, p_0)$.

By assuming that the source region is compact ($\partial/\partial t \ll c_0/\lambda$ where λ is the wavelength) and using a one-dimensional Green's function for an infinite tube [24], the expression of the pressure in the pipe segment 1 is obtained:

$$\begin{aligned} p_1'(x_1, t) = & -\frac{c_0}{2S} \int_S [\rho u_i]_{t^*} n_i \, \mathrm{d}S \\ & - \frac{1}{2S} \mathrm{sign}(x_1 - y_1) \int_S p'(y_1, t^*) n_1 \, \mathrm{d}S \\ & - \frac{1}{2S} \mathrm{sign}(x_1 - y_1) \int_S [\rho u_1 u_j]_{t^*} n_j \, \mathrm{d}S, \end{aligned} \tag{16}$$

where the brackets indicate that the value is taken at the retarded time $t^* = t - |x_1 - y_1|/c_0$ (with x_1 and y_1 the position of the observer and the source, respectively). More details about the derivation of the equation 16 is given below in the intermezzo. The surface S surrounding the control volume V used is shown in Figure 8. As there is no main flow, the method is in a linear approximation equivalent to a Kirchoff integral method.

This extraction method can be implemented as a post-processing of the numerical computations. One requires only the recording of the time history of the pressure $p'(t)$, the density $\rho(t)$, the velocity components $u_1(t)$ and $u_2(t)$ at the surface surrounding the region source. This surface consists of the surfaces S_1, S_1', S_2 and S_2' shown in Figure 8.

Intermezzo

Lighthill's equation (equation 12) is derived from the mass and momentum conservation laws.

Using Green's function formalism, Lighthill's analogy can be written in an integral form. The Green function is defined as the response $G(\boldsymbol{x}, t|\boldsymbol{y}, \tau)$, measured at a position $\boldsymbol{x}$ and time t, to a pulse sent from a source position $\boldsymbol{y}$ and time τ:

$$\frac{\partial^2 G}{\partial \tau^2} - c_0^2 \frac{\partial^2 G}{\partial y_i^2} = \delta(\boldsymbol{x} - \boldsymbol{y})\delta(t - \tau), \tag{17}$$

where $\delta(x)$ is the Dirac function.

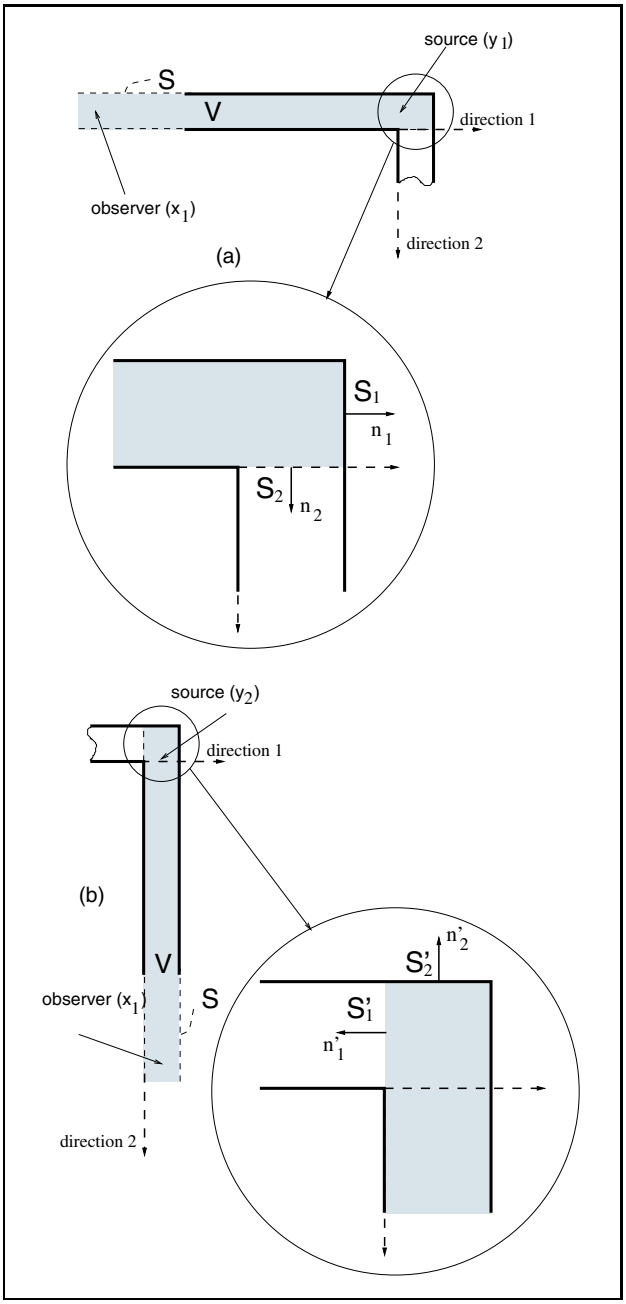

Figure 8. Volume V at which the integral method is applied for the determination of R_p (a), and T_p (b).

After some manipulations [25, 23], one obtains:

$$p'(\boldsymbol{x},t) = \int_{-\infty}^{t^+}\int_V T_{ij}\frac{\partial^2 G}{\partial y_i \partial y_j}\,\mathrm{d}\boldsymbol{y}\,\mathrm{d}\tau + \int_{-\infty}^{t^+}\int_S \rho u_i \frac{\partial G}{\partial \tau} n_i\,\mathrm{d}S\,\mathrm{d}\tau - \int_{-\infty}^{t^+}\int_S \frac{\partial G}{\partial y_i}(p'\delta_{ij} + \rho u_i u_j) n_j\,\mathrm{d}S\,\mathrm{d}\tau. \tag{18}$$

The general equation (18) is applied to a control volume V containing the entire domain in which we are interested. The volume V is bounded by a surface S with outwards normal n_i (Figure 8). The choice of V depends on the observer position $\boldsymbol{x}$ at which we want to determine the acoustical field. We chose the volume V as a half infinite pipe including the observer $\boldsymbol{x}$ and bounded by the bend (Figure 8).

We have the freedom to choose the Green function that we wish. We chose the low frequency approximation of the Green function for an infinite pipe (1-D Green's function [24]):

$$G(x_1,t|y_1,\tau) = \frac{c_0}{2S}H(t^* - \tau), \tag{19}$$

where $H(t)$ is the Heaviside function and t^* is the retarded time defined as:

$$t^* = t - \frac{|x_1 - y_1|}{c_0}. \tag{20}$$

By using the symmetry property ($\frac{\partial G}{\partial x_1} = -\frac{\partial G}{\partial y_1}$) of the Green function G, the general equation 18 can be written in the direction 1 (Figure 8):

$$p_1'(x_1,t) = \int_{-\infty}^{t^+}\left(-\frac{\partial}{\partial x_1}\right)\int_V T_{11}\frac{\partial G}{\partial y_1}\,\mathrm{d}\boldsymbol{y}\,\mathrm{d}\tau + \int_S \rho u_i \frac{\partial G}{\partial \tau} n_i\,\mathrm{d}S - \int_{-\infty}^{t^+}\int_S \frac{\partial G}{\partial y_1}(p'\delta_{1j} + \rho u_1 u_j) n_j\,\mathrm{d}S\,\mathrm{d}\tau. \tag{21}$$

In the far-field approximation ($x_1 \ll y_1$), only plane waves propagate and we can write:

$$\frac{\partial}{\partial x_1} \approx \frac{1}{c_0}\frac{\partial}{\partial t}. \tag{22}$$

By assuming that the source region is compact, equation 16 is deduced. The same method can be applied to the direction 2 to determine $p_2'(x_2,t)$.

3.3. Grid dependence of numerical computations

The grid-dependence of the numerical results has been studied by comparing the results obtained for three different grid refinements. In the interior of the numerical domain, the spatial discretization method is based on a cell-centered finite-volume method which is second-order accurate. The predicted coefficients of the scattering matrix $\mathcal{S}$ appear to behave as:

$$C_{exact} = C_{numerical} + O(\Delta x), \tag{23}$$

where $C_{numerical}$ represents either the calculated values of the amplitude or the phase of the reflection or transmission coefficients. C_{exact} is the extrapolated value or converged value. Δx is the cell width.

This corresponds to a first-convergence which might be due either to post-processing or a problem in the use of a first-order spatial discretization of the boundary conditions.

Computations were performed on three different grids. The fine grid had twice the refinement of the intermediate

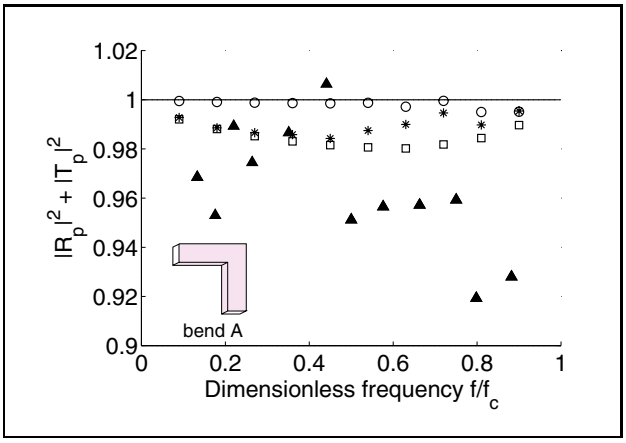

Figure 9. Bend A (2D-bend with a sharp inner edge and a sharp outer corner): Verification of the energy conservation (equation 5) as a function of the dimensionless frequency f/f_c. Comparison between the analytical solution (mode expansion truncated after 10 modes) (———); the experimental data of Lippert [8] (▲); 2-D Euler computations on a fine grid with 1-D extraction (□) and with the integral method (∗); the extrapolated or converged values deduced from equation 23 using a 1-D extraction (o).

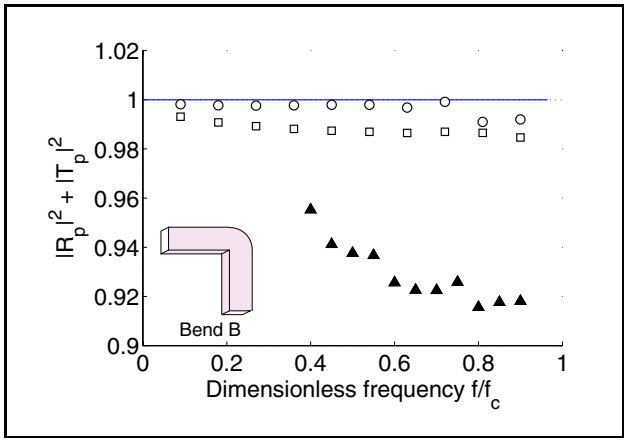

Figure 10. Bend B (2D-bend with a sharp inner edge and a rounded outer corner): Verification of the energy conservation (equation 5) as a function of the dimensionless frequency f/f_c. Comparison between the experimental data of Lippert [8] (▲; 2-D Euler computations with 1-D extraction (□); the extrapolated or converged values deduced from equation 23 (o).

grid in both x and y-directions. In the region marked out by the polygon $ABCDEF$ (Figure 6), the intermediate grid had 48 cells both in x (segment CD) and y-directions (segment AF). The number of cells was progressively decreased by a factor of two in the y-direction for upstream blocks and in the x-direction for downstream blocks.

The extrapolated values of the amplitude of the reflection and transmission coefficients have been deduced from numerical computations and the energy conservation law (equation 5) has been verified. Figures 9 and 10 show the results obtained for the bend with a sharp outer edge (bend A) and with a rounded outer corner (bend B), respectively. For the 2-D Euler calculations on the fine grid, the energy conservation is verified within 2%. The extraction by means of the integral method (Figure 9) provides here better results at high frequencies ($f/f_c > 0.5$). This is expected to be due to the more accurate description of the wave propagation in the integral method. Equation 5 is only verified within 8% by the experimental data of Lippert [8]. This indicates that the discrepancies between experimental and theoretical data (observed in Figures 2 and 3) are mainly due to experimental errors. In the next sections, only the numerical results obtained with the fine grid will be presented, as the numerical accuracy obtained is comparable to that of the experimental results presented in section 5.3.

4. Experimental study

In addition to the use of Lippert's data [8] for bends in pipes with square cross-section, we compared our numerical calculations with our own measurements for bends in pipes with circular cross-section. This section provides some information about the experimental procedure.

4.1. Bends

The bends were made in massive brass blocks with an accuracy of the order of $10\,\mu$m (wall roughness). The steel pipe diameter was $D = 0.03$ m and the pipe thickness was 5 mm. The wall roughness of the straight pipe segments was of the order of $0.1\,\mu$m.

4.2. Two-source method

The measurements of the scattering matrix coefficients (equation 2) by means of a two-source method were performed at the LAUM (Laboratoire d'Acoustique de l'Université du Maine). The method is described in detail by Ajello [15] and Durrieu [16].

Figure 11 shows a scheme of the experimental setup. Two sets of four microphones are placed at $x_{1\ell}$ ($\ell = 1,2,3,4$) upstream of the bend and at $x_{2\ell}$ ($\ell = 1,2,3,4$) downstream of the bend, respectively. The choice of four microphones at each side of the bend enables us to get accurate measurements in a broad range of frequencies ($30Hz \leq f \leq 1kHz$). The presence of anechoic terminations upstream and downstream of the bend suppresses the standing wave pattern and reduces the sensitivity of the measurements to errors. Two loudspeakers used as sources are placed respectively upstream and downstream of the bend. Using loudspeakers enables us to use an automatic source control. The sources are driven by a swept sine by means of the HP3565 analyzer. The air temperature is determined from acoustical measurements and is assumed to be constant during one sweep.

For a harmonic wave at the frequency f, the acoustical pressure $p'(x,t)$ and velocity $u'(x,t)$ in the pipe segments at each side ($i = 1,2$) of the bend are given by:

$$p'_i(x_{i\ell},t) = \left[p_i^+ \mathrm{e}^{-\mathrm{j}kx_{i\ell}} + p_i^- \mathrm{e}^{\mathrm{j}kx_{i\ell}}\right] \mathrm{e}^{2\mathrm{j}\pi ft}, \quad (24)$$

$$u'_i(x_{i\ell},t) = \frac{p_i^+ \mathrm{e}^{-\mathrm{j}kx_{i\ell}} - p_i^- \mathrm{e}^{\mathrm{j}kx_{i\ell}}}{\rho_0 c_0} \mathrm{e}^{2\mathrm{j}\pi ft}, \quad (25)$$

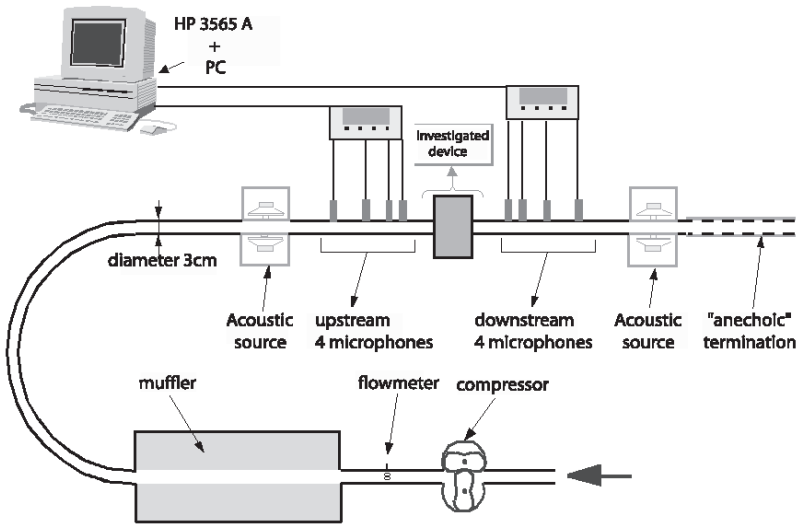

Figure 11. Scheme of experimental setup used for the two-source method measurements (LAUM – Laboratoire d'Acoustique de l'Université du Maine, Fr). The position of the microphones is $x_{12}-x_{11}=-0.100$ m, $x_{13}-x_{11}=-0.475$ m, $x_{14}-x_{11}=-1.072$ m upstream of the bend, and $x_{22}-x_{21}=0.100$ m, $x_{23}-x_{11}=0.475$ m, $x_{24}-x_{11}=1.072$ m downstream of the bend. For the bend with a sharp inner edge and a sharp outer corner $x_{11}=-0.4398$ m and $x_{21}=0.6621$ m. For the bend with a sharp inner edge and a rounded outer corner $x_{11}=-0.3953$ m and $x_{21}=0.6176$ m.

with k the wave number:

$$k=\frac{2\pi f}{c_0}-\mathrm{j}\alpha_0, \tag{26}$$

for $(\alpha_0 c_0/2\pi f)\ll 1$ and $j\equiv\sqrt{-1}$.

In the absence of a main flow ($\overline{u_1}=0$), the damping coefficient α_0 due to visco-thermal dissipation in the boundary layers at the pipe wall is approximated by Kirchhoff's formula [26]:

$$\alpha_0=\frac{2\pi f\delta_{ac}}{c_0 D}(1+\frac{\gamma-1}{\sqrt{P_r}}), \tag{27}$$

where $\gamma=1.4$ is the ratio of specific heats, $P_r=0.71$ is the Prandtl number and $\delta_{ac}=\sqrt{\nu/\pi f}$ is the thickness of the acoustic boundary layer. The kinematic viscosity of air is $\nu=1.51\times10^{-5}$ m^2/s at a room temperature of 293 K and at atmospheric pressure.

In the presence of a main flow as considered in part II [1], we used a fit of Hofmans [27] of the damping coefficient measured by Ronneberger [28] and Peters [29].

The pressure reflection coefficient $R_{pi}=p_i^-/p_i^+$ is deduced from measurement of the transfer function $H_{21}=p_i'(x_{i2})/p_i'(x_{i1})$ using the two-microphones method. The transmission coefficient $T_{p21}=p_2^+/p_1^+$ can be deduced from the value of the reflection coefficients R_{p1} and R_{p2}. In the absence of a main flow, only one measurement series is needed to determine the coefficients of the scattering matrix $\mathcal{S}$. The two independent acoustic states used in the determination of the coefficients of the scattering matrix (equation 2) are obtained using either the upstream or the downstream sound source. These two sets of measurements provide an independent check of the experimental accuracy by comparison of $|R_p^+|$ and $|T_p^+|$ with $|R_p^-|$ and $|T_p^-|$, respectively.

The two-source method is very convenient because it enables to measure the acoustic response of discontinuities in a broad range of frequencies. Most of the experimental results presented were performed at frequencies in the range 30 Hz $\leq f\leq$ 1 kHz. Typical accuracy of the data is 0.2% for both $|R_p^\pm|$ and $|T_p^\pm|$. Some data up to frequencies of 4 kHz will be presented. These data are, however, less accurate than low frequency data (30 Hz $\leq f\leq$ 1 kHz).

5. Results

5.1. Test case: 2-D bend with a sharp inner edge and a sharp outer corner

The acoustical response of a bend with a sharp inner edge and a sharp outer corner has been measured for pipes with square cross-sections by Lippert [8] for frequencies f up to the cut-off frequency f_c. His experimental data have been compared in Figure 2 with the results of an analytical model based on a mode expansion as proposed by Miles [7]. The results are also compared to the results of numerical computations based on the 2-D Euler equations.

Lippert's data [8] for the reflection and transmission coefficients $R_p=|R_p|exp(j\Phi_R)$ and $T_p=|T_p|exp(j\Phi_T)$ as a function of the dimensionless frequency f/f_c are shown in the Figures 12 and 13. The reference planes for determining the origin of the phases are the planes $x=0$ for Φ_R and $y=0$ for Φ_T, respectively, as shown in Figure 1.

The experimental results are compared to the results of the mode expansion truncated after ten modes and the results of numerical computations discussed in section 3.

As explained in section 1, the numerical data are obtained in two different ways: by means of the 1-D extraction procedure and the integral method.

The two different extraction procedures (1-D extraction and integral method) give similar results except at frequencies near the cut-off frequency at which the phase differs slightly from the theoretical data. The theory predicts quite accurately the experimental data of Lippert [8].

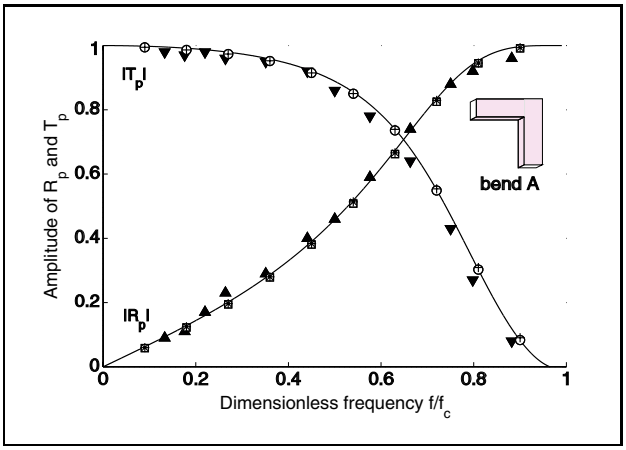

Figure 12. Bend A (2D-bend with a sharp inner edge and a sharp inner corner): Amplitude of the reflection and transmission coefficients as a function of the dimensionless frequency f/f_c. Comparison between the analytical solution (mode expansion truncated after 10 modes): ———; the experimental data of Lippert [8]: ▲, ▼; 2-D Euler computations with 1-D extraction (□, o) and with the integral method (∗, +).

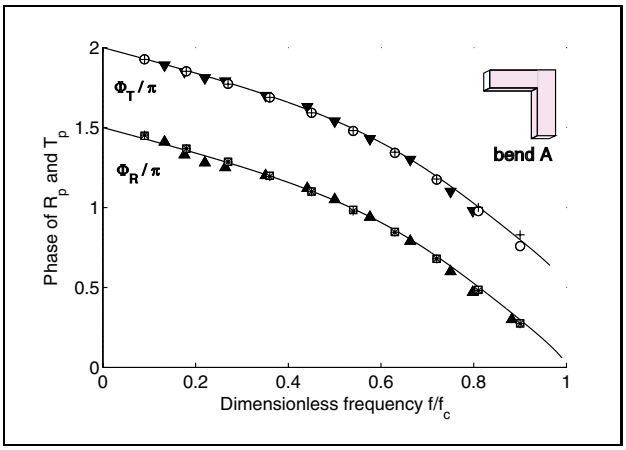

Figure 13. Bend A (2D-bend with a sharp inner edge and a sharp inner corner): Phase of the reflection and transmission coefficients as a function of the dimensionless frequency f/f_c. Comparison between the analytical solution (mode expansion truncated after 10 modes): ———; the experimental data of Lippert [8]: ▲, ▼; 2-D Euler computations with 1-D extraction (□, o) and with the integral method (∗, +).

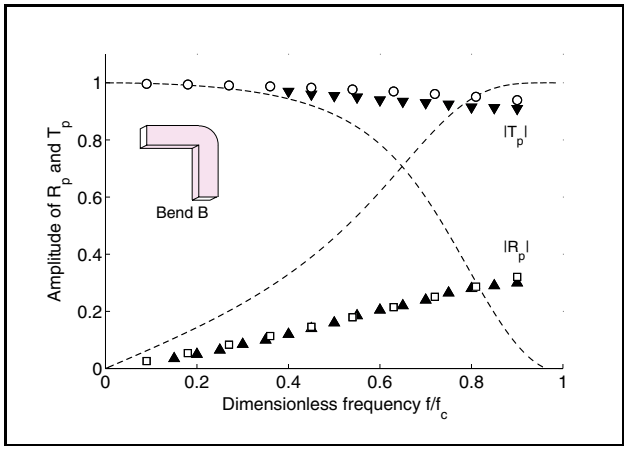

Figure 14. Bend B (2D-bend with a sharp inner edge and a rounded outer corner): Amplitude of the reflection and transmission coefficients in terms of the dimensionless frequency f/f_c. Comparison between experimental data (Lippert [8]): ▲, ▼; and Euler computation data: □, o. For reference, the magnitude of the coefficients obtained for the bend A (sharp outer corner) is also plotted: — — —.

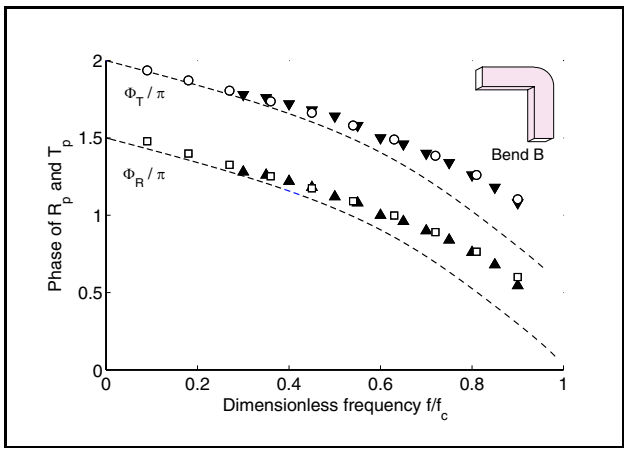

Figure 15. Bend B (2D-bend with a sharp inner edge and a rounded outer corner): Phase of the reflection and transmission coefficients in terms of the dimensionless frequency f/f_c. Comparison between experimental data (Lippert [8]): ▲, ▼; and Euler computation data: □, o. For reference, the phase of the coefficients obtained for the bend A (sharp outer corner) is also plotted: — — —.

5.2. 2-D bend with a sharp inner edge and a rounded outer corner

The case of a 2-D 90° bend with a sharp inner edge and a rounded outer corner (bend B, Figure 1) has also been studied by Lippert [8]. He used the bend with a sharp inner edge and a sharp outer corner (bend A, Figure 1) to which he added a sheet of brass with a radius equal to the height of the duct. The space left between the sheet and the outer corner of the bend was filled with sand.

In Figures 14 and 15, the experimental data of Lippert [8] are compared with results of 2-D Euler computations. The agreement is fair. The behavior is quite different from that of the bend with a sharp outer corner (bend A, Figure 1). The amplitude of the transmission coefficient T_p remains greater than 0.9 (up to $f/f_c = 1$), while the amplitude of the reflection coefficient R_p remains lower than 0.35. The measured amplitude of the transmission coefficient is lower than the prediction of the 2-D Euler computations. Verification of the energy conservation shown in Figure 10, indicates a problem with the experimental data.

5.3. Comparison between 2-D and 3-D data

The acoustic response of the bends with a sharp inner edge and either a sharp or rounded outer corner in pipes with circular cross-section (bends C and D, Figure 1) has been measured. For these configurations, the flow is not planar.

The experimental method used is the two-source method described in section 2.

Figures 16 and 17 present the comparison between the 2-D analytical and 3-D experimental data obtained for bends with a sharp inner edge and a sharp outer corner (bends A and C, Figure 1), and for bends with a sharp inner edge and a rounded outer corner (bends B and D, Figure 1). The comparison is made for frequencies f up to 1 kHz, this corresponds to dimensionless frequencies f/f_c up to 0.15. In Figure 16, only the 2-D analytical solution is shown because 2-D experimental data of Lippert [8] are not available for such low frequencies. In Figure 17, a fit of the numerical data presented in Figure 14 and 15 was used. In first approximation, for bends with a sharp inner edge and a sharp outer corner (bends A and C), we see that 2-D and 3-D data correspond to each other for equal dimensionless frequencies f/f_c.

Note that the excellent agreement between the measured values of T_p^+ and T_p^-, obtained from two independent measurement series (one with each source), indicates a typical accuracy of 0.2%. The small deviation of 0.5% at the frequency $f/f_c = 0.15$ between theory and experiment is therefore considered to be significant. This is expected to be due to visco-thermal losses at the bend. The damping coefficient α_0 calculated by means of Kirchhoff's formula [29] (equation 27) for a straight pipe varies, for the frequency range considered, in the range $3 \times 10^{-4} < \alpha_0 D < 2 \times 10^{-3}$. Hence, the observed dissipation in the bend is of the order of magnitude of the visco-thermal damping for a tube length of one diameter. In the case of the bend with a sharp inner edge and a sharp outer corner (bend A, Figure 1), the bend center line has a length of one diameter D. The dissipation is about a factor of three higher than $\alpha_0 D$. This is expected to be due to the strong viscous dissipation around the inner edge of the bend at which the acoustical flow is singular (Morse & Ingard [30]).

The results obtained by means of Nederveen's theory [13] (section 2.3) do not give a better prediction of the coefficients of the scattering matrix $\mathcal{S}$ in our case. Figure 17 shows that for $f/f_c \leq 0.15$, the behavior of the 3D-bend with a rounded outer corner (bend D, Figure 1) does not at all agree with the behavior of the 2D-bend (bend B, Figure 1) nor the predictions of Nederveen's theory [13].

An additional series of measurements was performed on the bend with a sharp inner edge and a rounded outer corner (bend D, Figure 1) at higher frequencies (up to $f/f_c = 0.6$). The results are presented in Figure 18. Assuming that 2-D and 3-D data correspond to each other for equal dimensionless frequencies f/f_c, appears not to be a good approximation in the case of such a bend with a sharp inner edge and a rounded outer corner. Our measurements on the bend D (Figure 1) with circular pipe cross-sections deviate indeed from the 2-D experimental data of Lippert [8] and the 2-D numerical simulations. The intuitive approach of Nederveen [13] to deduce 3-D data from 2-D data also fails in that case (section 5.2, Figure 15). It appears that, in the range of frequencies considered, the acoustical response of bends with a sharp inner edge in pipes with circular cross-sections is almost independent of

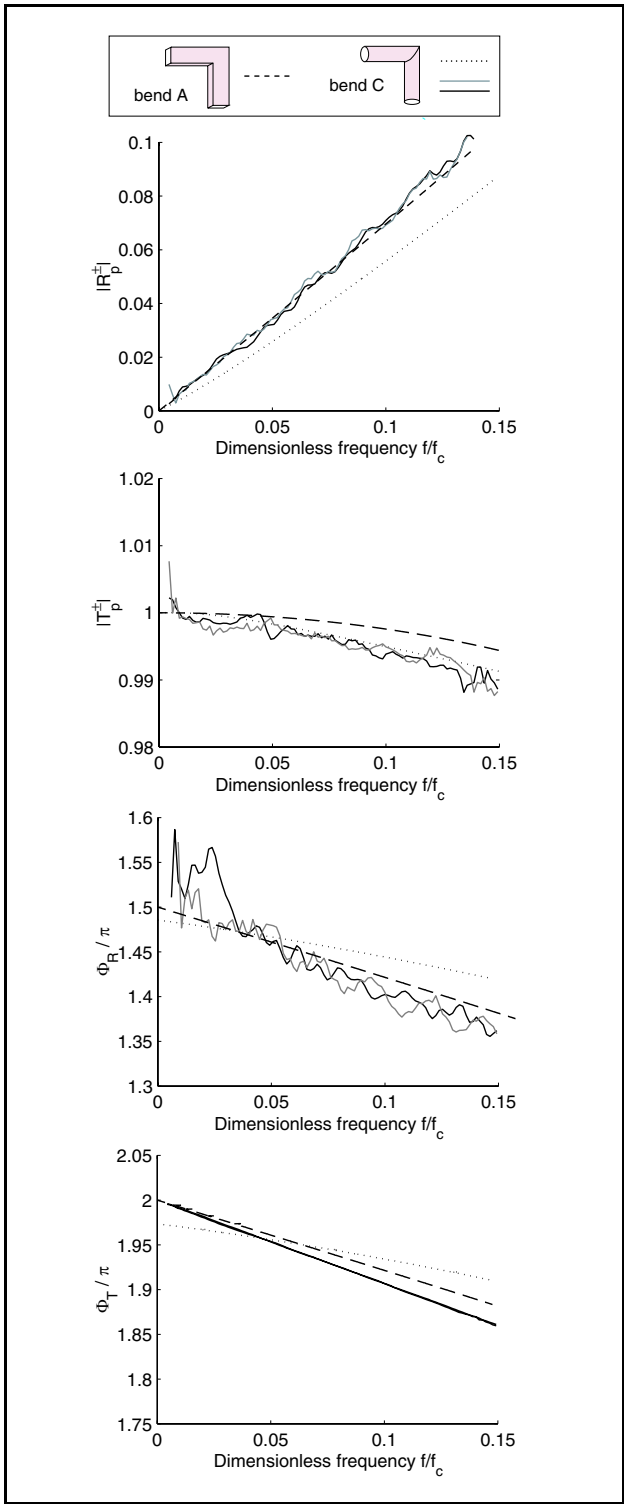

Figure 16. Bends A and C (sharp inner edge and sharp outer corner): Comparison of 2-D theory (– – – –) and 3-D experimental data (R_p^+, T_p^+ ——— and R_p^-, T_p^- ———) for equal dimensionless frequencies f/f_c and without main flow ($\overline{u_1} = 0$). The results of the decomposition of the bend in parallel thin layers (as proposed by Nederveen [13] are also shown (.....).

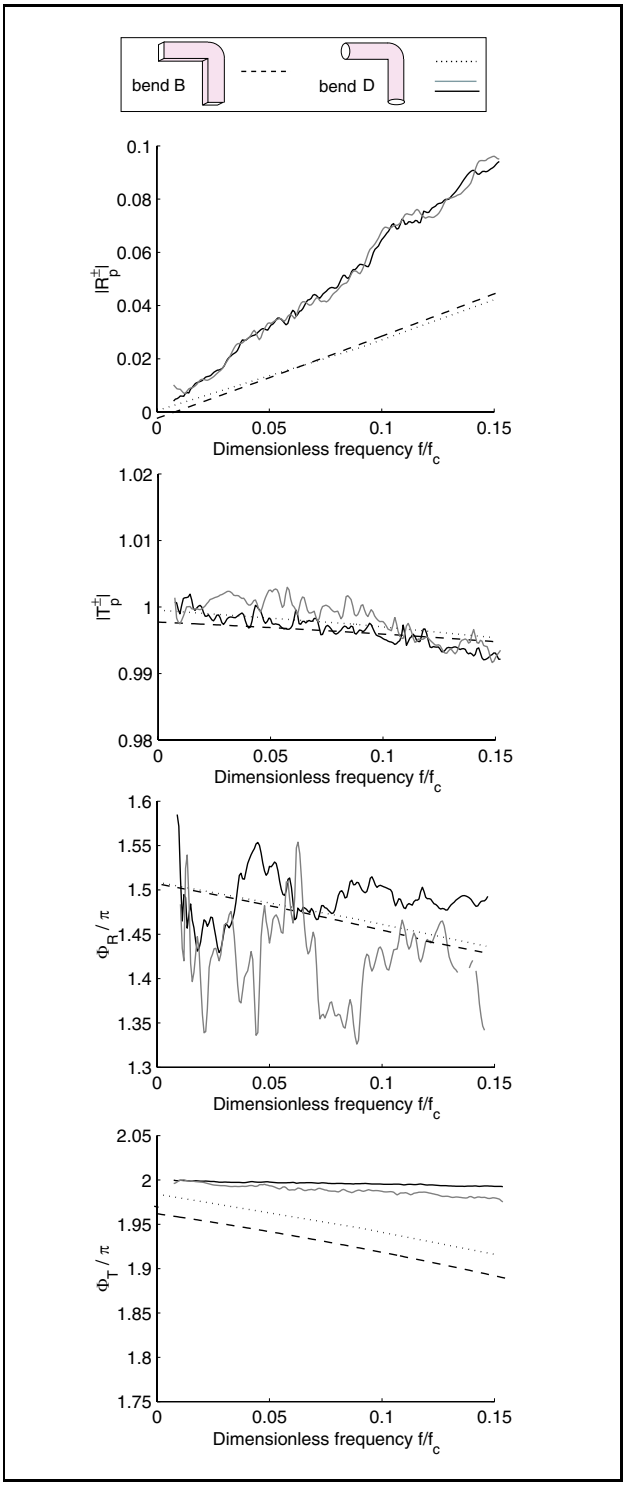

Figure 17. Bends B and D (sharp inner edge and rounded outer corner): Comparison of 2-D data (– – – – –) and 3-D experimental data (R_p^+, T_p^+ ——— and R_p^-, T_p^- ———) for equal dimensionless frequencies f/f_c and without main flow ($\overline{u_1} = 0$). The 2-D data are obtained by using a fit of the numerical data showed at Figure 14 and 15. The results of the decomposition of the bend in parallel thin layers (as proposed by Nederveen [13] are also shown (.....).

the shape of the outer corner. This is a rather unexpected result for which we do not have any explanation.

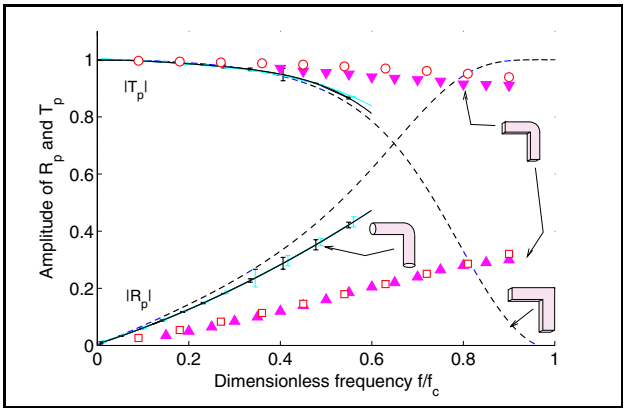

Figure 18. Bends B and D (sharp inner edge and rounded outer corner) without main flow ($\overline{u_1} = 0$): Comparison of 2-D numerical data (□, o) with 2-D experimental data (▲, ▼) of Lippert [8] and a fit of 3-D experimental data obtained by means of the two-source method (———) with errorbars). The results are shown in terms of the dimensionless frequency f/f_c. The 2-D modal theory for the sharp bend with a sharp outer corner is also shown (– – – –).

6. Conclusions

The results of analytical techniques and a numerical method for the 2-D Euler equations have been compared with experimental data for the acoustical response of 90° bends with a sharp inner edge. The quality of acoustical predictions by means of such numerical computations has been verified. Furthermore, a dramatic effect of the shape of the bend on the difference between the response of bends in pipes with square cross-sections compared to that in pipes with circular cross-sections has been observed.

In the case of a 90° bend with a sharp inner edge and a sharp outer corner, the 2-D numerical simulations accurately predict the available 2-D experimental data from the literature [8] and the analytical prediction based on a mode expansion [7]. The 2-D analytical and numerical predictions also agree with experimental data for pipes with circular cross-sections measured by means of a two-source method for equal ratio f/f_c of the frequency f and the cut-off frequency f_c.

The acoustical response of a 90° sharp bend with a rounded outer corner has also been studied. Numerical simulations based on the 2-D Euler equations accurately predict the 2-D experimental data from the literature [8]. For equal dimensionless frequencies f/f_c, the comparison of 2-D numerical and experimental data with 3-D experimental results obtained by means of a two-source method shows an unexpected behavior. Measurements show that the acoustical response of a sharp bend with a rounded outer corner in pipes with circular cross-sections is close to that of a bend with a sharp inner edge and a sharp outer corner. The acoustical response of the bend in pipes with circular cross-section seems independent of the shape of the outer corner. This is quite different from the behavior of the bends in pipes with square cross-sections. An attempt to deduce the reflection and transmission coeffi-

cients in a 3D-bend from the measured coefficients in a 2D-bend has be done by decomposing the circular cross-section of the 3D-bend into parallel thin independent rectangular layers as proposed by Nederveen [13]. At low frequencies, the calculated coefficients are similar to the measured coefficients for a 2D-bend. This method does however not explain the unexpected behavior of the 3-D bend with a rounded outer corner found in the present measurements.

Acknowledgement

This work has been carried out within the framework of the European Project 'Flow Duct Acoustics' (FLODAC, BRPR CT97-10394).

References

[1] S. Dequand, S. J. Hulshoff, Y. Aurégan, J. Huijnen, L. J. van Lier, A. Hirschberg: Acoustics of 90 Degree Sharp Bends. Part II: Low-Frequency Aeroacoustical Response. Acta Acustica united with Acustica **90** (2004) to appear.

[2] W. Rostafinski: On Propagation of Long Waves in Curved Ducts. J. Acoust. Soc. Am. **52** (1972) 1411–1420.

[3] W. Rostafinski: Analysis of Propagation of Waves of Acoustic Frequencies in curved ducts. J. Acoust. Soc. Am. **56** (1974) 11–15.

[4] W. Rostafinski: Monograph on Propagation of Sound Waves in Curved Ducts. NASA - reference publication 1248 (1991).

[5] A. Cummings: Sound Transmission in Curved Duct Bends. J. Sound Vib. **35** (1974) 451–477.

[6] S. Félix, V. Pagneux: Sound Propagation in Rigid Bends: a Multimodal Approach. J. Acoust. Soc. Am. **110 (3)** (2001) 1329–1337.

[7] J. W. Miles: The Diffraction of Sound due to Right-angled Joints in Rectangular Tubes. J. Acoust. Soc. Am. **19 (4)** (1947) 572–579.

[8] W. K. R. Lippert: Wave Transmission around Bends of Different Angles in Rectangular Ducts. Acustica **5** (1955) 274–278.

[9] C. Thompson: Linear Inviscid Wave Propagation in a Waveguide having a Single Boundary Discontinuity. Part II: Application. J. Acoust. Soc. Am. **75** (1984) 356–362.

[10] J. C. Bruggeman: The Propagation of Low-Frequency Sound in a Two-Dimensional Duct System with T-joints and Right Angle Bends: Theory and Experiments. J. Acoust. Soc. Am. **82 (3)** (1987) 1045–1051.

[11] D. H. Keefe, A. H. Benade: Wave Propagation in Strongly Curved Ducts. J. Acoust. Soc. Am. **74** (1983) 320–332.

[12] S. Félix, V. Pagneux: Multimodal Analysis of Acoustic Propagation in Three-dimensional Bends. Wave Motion **36 (2)** (2002) 157–168.

[13] C. J. Nederveen: Influence of a Toroidal Bend on Wind Instrument Tuning. J. Acoust. Soc. Am. **104 (3)** (1998) 1616–1626.

[14] M. Åbom: Measurement of the Scattering Matrix of Acoustical Two Ports. Mechanical Systems and Signal Processing **5** (1991) 89–104.

[15] G. Ajello: Mesures acoustiques dans les guides d'ondes en présence d'écoulement: mise au point d'un banc de mesures, application à des discontinuités. Dissertation. Université du Maine, Le Mans, 1997.

[16] P. Durrieu, G. Hofmans, G. Ajello, R. Boot, Y. Aurégan, A. Hirschberg, M. Peters: Quasi-Steady Aero-Acoustic Response of Orifices. J. Acoust. Soc. Am. **110** (2001) 1859–1872.

[17] J. W. M. Gijrath, B. T. Verhaar, J. C. Bruggeman: Prediction Model for Broadband Noise in Bends. Proceedings of the 7th international conference on Flow-Induced Vibration-FIV2000, Lucerne, Switzerland, 19-22 June 2000.

[18] S. Nygård: Low Frequency Sound in Duct Systems. Tech. Rept. The Marcus Wallenberg Laboratory for Sound and Vibration Research, Royal Institute of Technology, Sweden (ISSN 1103-470X, ISRN KTH/FKT/L 00/57), 2001.

[19] S. W. Rienstra, A. Hirschberg: An Introduction to Acoustics. Tech. Rept. Eindhoven University of Technology, The Netherlands, May 2001.

[20] S. Dequand: Duct Aeroacoustics: from Technological Applications to the Flute. Dissertation. Technische Universiteit Eindhoven (Nl) and Université du Mans (Fr), 2001.

[21] S. J. Hulshoff: EIA: an Euler Code for Internal Aeroacoustics. Part 1: Method Description and User's Guide. Tech. Rept. Eindhoven University of Technology (Nl), 2000.

[22] S. Dequand: EIA: an Euler Code for Internal Aeroacoustics. Part 2: Example Computations. Tech. Rept. Eindhoven University of Technology (Nl), 2000.

[23] M. Goldstein: Aeroacoustics. Mc Graw-Hill, New-York, 1976.

[24] G. C. J. Hofmans: Vortex Sound in Confined Flows. Dissertation. Technische Universiteit Eindhoven, 1998.

[25] D. Crighton, A. Dowling, J. F. Williams, M. Heckl, F. Leppington: Modern Methods in Analytical Acoustics. Springer-Verlag, London, 1992.

[26] A. D. Pierce: Acoustics: An introduction to its physical principles and applications. Acoustical Society of America Edition, 1989.

[27] G. C. J. Hofmans, R. J. J. Boot, P. P. J. M. Durrieu, Y. Aurégan, A. Hirschberg: Aeracoustic Response of a Slit-Shaped Diaphragm in a Pipe at Low Helmholtz Number. Part 1: Quasi-Steady Results. J. Sound Vib. **244 (1)** (2001) 35–56.

[28] D. Ronneberger, C. Ahrens: Wall Shear Stress caused by Small Amplitude Perturbations of Turbulent Boundary Layer Flow: an Experimental Investigation. J. Fluid. Mech. **83** (1977) 433–464.

[29] M. C. A. M. Peters, A. Hirschberg, A. J. Reijnen, A. P. J. Wijnands: Damping and Reflection Coefficient Measurements for a Pipe at Low Mach and Low Helmholtz Numbers. J. Fluid Mech. **256** (1993) 499–534.

[30] Morse, Ingard: Theoretical acoustics. Mc Graw Hill, 1967.